Insights into the Reaction Mechanism of Soluble Epoxide Hydrolase from Theoretical Active Site Mutants

Kathrin H. Hopmann and Fahmi Himo*

Department of Theoretical Chemistry, School of Biotechnology, Royal Institute of Technology, AlbaNova University Center, SE-106 91 Stockholm, Sweden

Received: June 20, 2006; In Final Form: August 16, 2006

Density functional theory calculations of active site mutants are used to gain insights into the reaction mechanism of the soluble epoxide hydrolases (sEHs). The quantum chemical model is based on the X-ray crystal structure of the human soluble epoxide hydrolase. The role of two conserved active site tyrosines is explored through in silico single and double mutations to phenylalanine. Full potential energy curves for hydrolysis of (1*S*,2*S*)-β-methylstyrene oxide are presented. The results indicate that the two active site tyrosines act in concert to lower the activation barrier for the alkylation step. For the wild-type and three different tyrosine mutant models, the regioselectivity of epoxide opening is compared for the substrates (1*S*,2*S*)-β-methylstyrene oxide and (*S*)-styrene oxide. An additional part of our study focuses on the importance of the catalytic histidine for the alkylation half-reaction. Different models are presented to explore the protonation state of the catalytic histidine in the alkylation step and to evaluate the possibility of an interaction between the nucleophilic aspartate and the catalytic histidine.

Introduction

Epoxide hydrolases (EHs) convert epoxides to their corresponding vicinal diols. EHs are found in a variety of different organisms and are involved in different functions such as detoxification and metabolism.[1] The known EHs belong to different classes, the most prominent of which is the α/β-hydrolase fold EHs. Besides the characteristic α/β-hydrolase fold, these EHs also exhibit several conserved residues including a catalytic triad and the oxyanion hole motif HG*X*P.[2−7] Structural and biochemical data indicate that the different α/β-hydrolase fold EHs operate through the same catalytic mechanism.[3−14] A well-known member of this family is the mammalian soluble epoxide hydrolase (sEH), which is involved in detoxification of xenobiotic compounds, but also endogenous epoxides arising from lipid metabolism are among the substrates.[15,16]

Experimental data has given a detailed picture of the reaction mechanism of α/β-fold hydrolase EHs.[8−13,17] Epoxide hydrolysis is mediated by the catalytic triad Asp/Glu−His−Asp (Scheme 1), which also is known from the haloalkane dehalogenases. Nucleophilic attack of an aspartate residue of the catalytic triad on the epoxide substrate results in formation of a covalent enzyme−substrate intermediate. This step is referred to as the alkylation half-reaction. In the subsequent hydrolytic half-reaction, the histidine residue of the catalytic triad activates a water molecule, which attacks the ester bond between the nucleophilic aspartate and the substrate. A conserved oxyanion hole is important to stabilize the formed tetrahedral intermediate. The final diol product is obtained through dissociation of the tetrahedral intermediate.

In addition to the catalytic triad, it has been proposed that the reaction mechanism involves an epoxide-activating residue, which hydrogen-bonds to the epoxide and facilitates ring opening.[7] The nature of this epoxide-activating residue was a matter of speculation for some time.[9−12] Mutational studies as well as structural data clearly identified two tyrosines as the likely hydrogen bond/proton donors (Tyr465 and Tyr381 in human sEH).[3−6,18,19] In all five known crystal structures of α/β-hydrolase fold EHs, analogues of these two tyrosines are found in perfect position for substrate binding and activation.[3−6,14,20]

We have very recently investigated the full reaction mechanism for soluble epoxide hydrolase using quantum chemical calculations.[21] The model was based on the X-ray crystal structure of human sEH and consisted of 98 atoms.[14] An inhibitor found in the crystal structure was manually replaced with the substrate (1*S*,2*S*)-β-methylstyrene oxide (MSO) (the resulting quantum chemical model will hereafter be referred to as the wild-type (WT) model). Epoxide opening and hydrolysis of MSO with the WT model occurred in several steps.[21] The alkylation half-reaction was found to comprise two steps. In the alkylation transition state (TSa), the covalent enzyme substrate intermediate (CI) is formed through nucleophilic attack of Asp333 on the epoxide. The calculated barrier for attack at C1 of MSO is 7.8 kcal/mol. Following alkylation, a proton is transferred from Tyr465 to the former epoxide oxygen in a distinct step. It was discussed that it is possible that the calculated stepwise reaction is an artifact of our chemical model.[21] Recent experimental results, however, support a reaction mechanism in which epoxide protonation does not occur in concert with epoxide opening.[22] The hydrolytic half-reaction was shown to occur in two steps.[21] In the first step, His523 acts as a general base, activating the catalytic water molecule. The transition state for water attack (TSw) on the covalent enzyme−substrate intermediate has a computed barrier of 18.1 kcal/mol. A tetrahedral intermediate is formed, which is stabilized through hydrogen bonding to the Trp334 and Phe265 backbone nitrogens. The two hydrogen bonds comprise what is known as the oxyanion hole. The formed tetrahedral intermediate was found to lie in a shallow minimum, 1 kcal/

* Corresponding author. E-mail: himo@theochem.kth.se.

10.1021/jp063830t CCC: $33.50
Published on Web 10/03/2006

SCHEME 1. SEH Reaction Mechanism (Residue Numbering as in Human sEH)

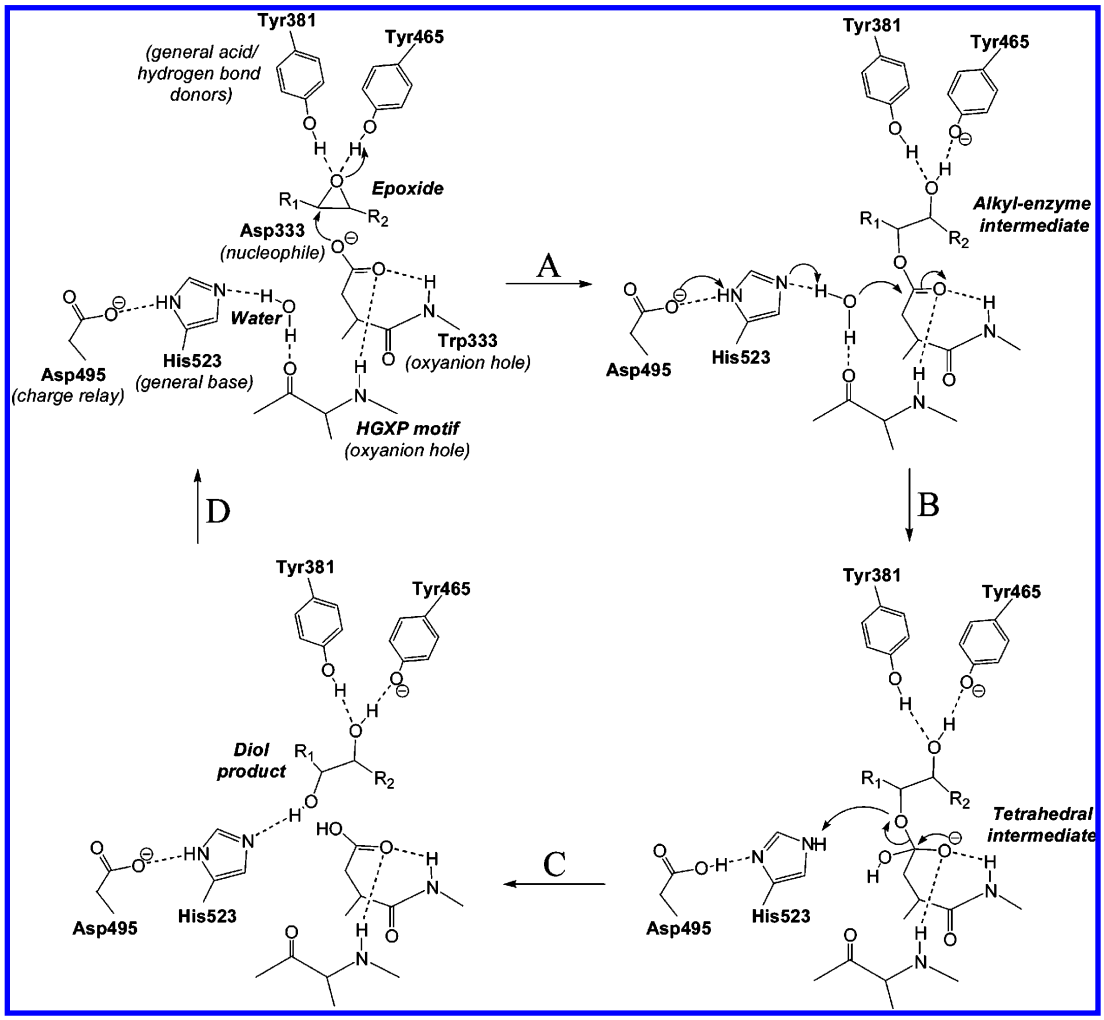

mol lower than the TS for its formation (TSw) and 5.5 kcal/mol lower than the TS for its dissociation (TSd).[21] In the second step of the hydrolytic half-reaction, the covalent bond between Asp333 and the substrate is broken, resulting in formation of the diol product. In the calculations, the dissociation of the covalent enzyme−substrate bond is coupled to simultaneous proton transfer from His523 to the emerging oxyanion of the diol.[21] In addition to the calculations of the reaction mechanism, we also considered the regioselectivity of sEH-mediated MSO hydrolysis, where we showed that alkylation at the C2 position has a barrier of 11.0 kcal/mol, which is 3.2 kcal/mol higher than the barrier for attack at the benzylic position (C1).[21] The observed regioselectivity for MSO is in good agreement with experimentally observed regioselectivities for different epoxide hydrolases.[23−25]

In the present study, we extend our investigations of the reaction mechanism of sEH by exploring how mutations of the active site tyrosines Tyr381 and Tyr465 to phenylalanines affect the energetics of the reaction. Quantum chemical models of both the single mutations, Tyr381Phe and Tyr465Phe, and the double mutation, Tyr381Phe/Tyr465Phe, were prepared and the potential energy curves were calculated. The effect of the tyrosine mutations on the regioselectivity of epoxide opening is addressed for different substrates. Additionally, we have investigated the role of the catalytic histidine residue in the alkylation half-reaction. A proposed protonation of His523 at Nϵ during the alkylation step is also addressed.

The theoretical method employed in the calculations is the hybrid density functional theory method of B3LYP. This computational strategy has proven successful for investigation of a variety of enzymatic reaction mechanisms.[26] The studied models have a size of up to 98 atoms, which is quite large for quantum chemical calculations, but still quite small for an enzyme active site. One interesting question in this context is whether it is possible to model effects of mutations making use of these relatively small models.

Computational Details

The calculations were performed with the hybrid density functional theory method B3LYP,[27] as implemented in Gaussian03.[28] Geometries were optimized at the B3LYP/6-31G(d,p) level. During the optimization, certain atoms were fixed to their crystallographically observed positions (indicated by asterisks in the figures below). Single point calculations on the optimized structures were performed with the triple-ζ basis set, 6-311+G(2d,2p), to obtain more accurate energies. To estimate solvation effects of the rest of the enzyme that is not included in the quantum cluster, single point calculations on the optimized geometries were performed with the conductor-like polarizable continuum model (CPCM)[29] at the B3LYP/6-31G(d,p) level. The CPCM model assumes that the surroundings can be represented as a continuous homogeneous medium with a dielectric constant ϵ. In our calculations, the default cavity UAO was used. The dielectric constant was set to $\epsilon = 4$, which is the standard value used in modeling the effect of protein surroundings. In evaluation of the results, it should be kept in mind that the PCM approach gives only an approximate estimate of the solvation

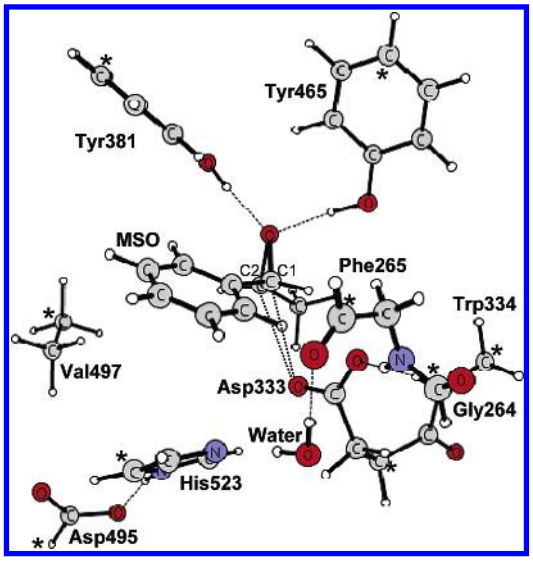

Figure 1. Quantum chemical model of human sEH (optimized reactant of the wild-type (WT) model). In this and all other figures, asterisks indicate atoms kept fixed to their crystallographically observed positions in calculations.

effect of the parts of the protein that are not included in the quantum chemical model. To confirm the nature of the stationary points and to calculate zero point vibrational effects, frequency calculations were performed on the optimized geometries at the B3LYP/6-31G(d,p) level. The stationary points should have only positive eigenvalues for minima and one negative eigenvalue (imaginary frequency) for transition states. Fixing of some of the atoms resulted in a few small negative eigenvalues on the order of -10 to -20 cm^{-1}, which does not influence the results.

Quantum Chemical Model. The chemical model is based on the X-ray crystal structure of human sEH (PDB 1VJ5),[14] as in our previous investigation.[21] The model is composed of the Asp495−His523−Asp333 catalytic triad, the two tyrosines Tyr381 and Tyr465, parts of the oxyanion hole residues Trp334, Phe265, and Gly264, a crystallographically observed water molecule, and parts of Val497 (Figure 1). In the human sEH X-ray crystal structure, the inhibitor *N*-cyclohexyl-*N*'-(iodophenyl)urea (CIU) is observed in the position where the substrate is suggested to bind.[14] In our model, the CIU inhibitor was manually replaced with (1*S*,2*S*)-β-methylstyrene oxide (MSO),[21] which is a substrate of human sEH and several rodent sEHs.[25] The (*S*)-styrene oxide (SSO) substrate, used in the regioselectivity calculations, has the same structure as MSO, except that the methyl group on C2 has been replaced with a hydrogen atom.

In the quantum chemical model shown in Figure 1 (referred to as the wild-type (WT) model, which has a total of 98 atoms), the tyrosine residues are modeled as phenols. To model the Tyr → Phe mutants, the hydroxyl group of the phenols was replaced with a hydrogen atom. The phenylalanine residues of the mutants are thus modeled as benzene rings. Models for both single mutants, Tyr381Phe and Tyr465Phe, were prepared as well as for the Tyr381Phe/Tyr465Phe double mutant. The mutant models are referred to as Y381F, Y465F, and Y381F/Y465F, respectively.

To study the role of His523, small variations in the WT model were performed. Two models were prepared, in both of which His523 is protonated at Nϵ, as opposed to the WT model, where the His523 Nϵ is unprotonated. The first model, denoted H523NϵH, is lacking the catalytic water molecule, whereas in the second model, denoted H523NϵH−H_2O, the water is present. Both models have an overall charge of -1. An additional model excludes Asp495, His523, and the catalytic water molecule. This model has also an overall charge of -1 and will in the following be referred to as NoHis523.

Results and Discussion

A. Geometries of Single and Double Tyrosine Mutants. All soluble epoxide hydrolases contain two conserved tyrosine residues, that in X-ray crystallographic studies have been shown to be located in the EH active site.[3,4,5,14,32] For several EHs, single and double Tyr → Phe mutants have been studied experimentally to analyze the importance of the conserved tyrosine residues for the epoxide hydrolysis reaction.[18,19,30,32] Significant differences in alkylation rates compared to the wild-type enzymes were observed in all cases, indicating a role of the tyrosine residues in epoxide activation.[18,19,30,32] We were interested in investigating if theoretical modeling of tyrosine mutants of the human soluble epoxide hydrolase (sEH) could provide insight into the role of the active site tyrosines and if similar effects would be obtained as those observed experimentally for the above EHs.

Two single Tyr → Phe mutant models of human sEH were prepared by changing the phenol groups in the previously presented WT model[21] to phenyl instead. It was assumed that the tyrosine mutations would not result in significant changes in the positions of the residues. This seems to be a reasonable assumption for a Tyr → Phe mutation because large parts of the side chains are identical. For mutations that result in more significant structural changes, it might be necessary to obtain structural data to validate the position of a mutated residue. The single tyrosine mutant models will here be referred to as Y381F and Y465F, respectively. For both Y381F and Y465F, the full reaction of (1*S*,2*S*)-β-methylstyrene oxide (MSO) hydrolysis was studied. Also, a double mutant model, Y381F/Y465F, was studied theoretically. It was of particular interest to us to see how activation barriers and geometric parameters would be affected by the single and double mutations. In Figure 2, the optimized alkylation transition state (TSa) structures for attack at C1 of MSO for all models are compared (the reactants for the mutant models can be found in Supporting Information, Figures S1A, S2A, and S3A). Table 1 compares the key distances of the optimized transition state structures of the WT and the mutant models. The two single mutants yield very similar bond distances. At the alkylation TS, the critical distance (r1) between the Asp333 Oδ2 and the benzylic carbon (C1) of MSO is 2.15 and 2.16 Å for Y381F and Y465F, respectively (Table 1, Figure 2). In the WT model, the corresponding distance is 2.29 Å, while in the Y381F/Y465F double mutant model, it is considerably shorter, only 1.97 Å. The O−C distance (r2) of the partially opened epoxide is 1.89 Å in the WT model, 1.97 Å in both single mutant models, and 2.01 Å in the double mutant. The distance (r3) between the epoxide oxygen and the hydroxy proton of the remaining tyrosine is 1.49 and 1.55 Å for Y381F and Y465F, respectively. In the WT model, the distances are 1.61 and 1.66 Å (Table 1, Figure 2). In the WT model, the alkylation half-reaction occurs in two steps, with the nucleophilic attack on the substrate first, followed by proton transfer from Tyr465 to the epoxide oxygen as a separate step. Interestingly, for both single mutants, alkylation and epoxide protonation occur concertedly. This difference can be explained with the number of hydrogen bonds to the epoxide. In the WT model, the oxyanion of the substrate is stabilized by two hydrogen bonds, and epoxide opening can thus occur without proton transfer. In the single mutants, one of the hydrogen bonds

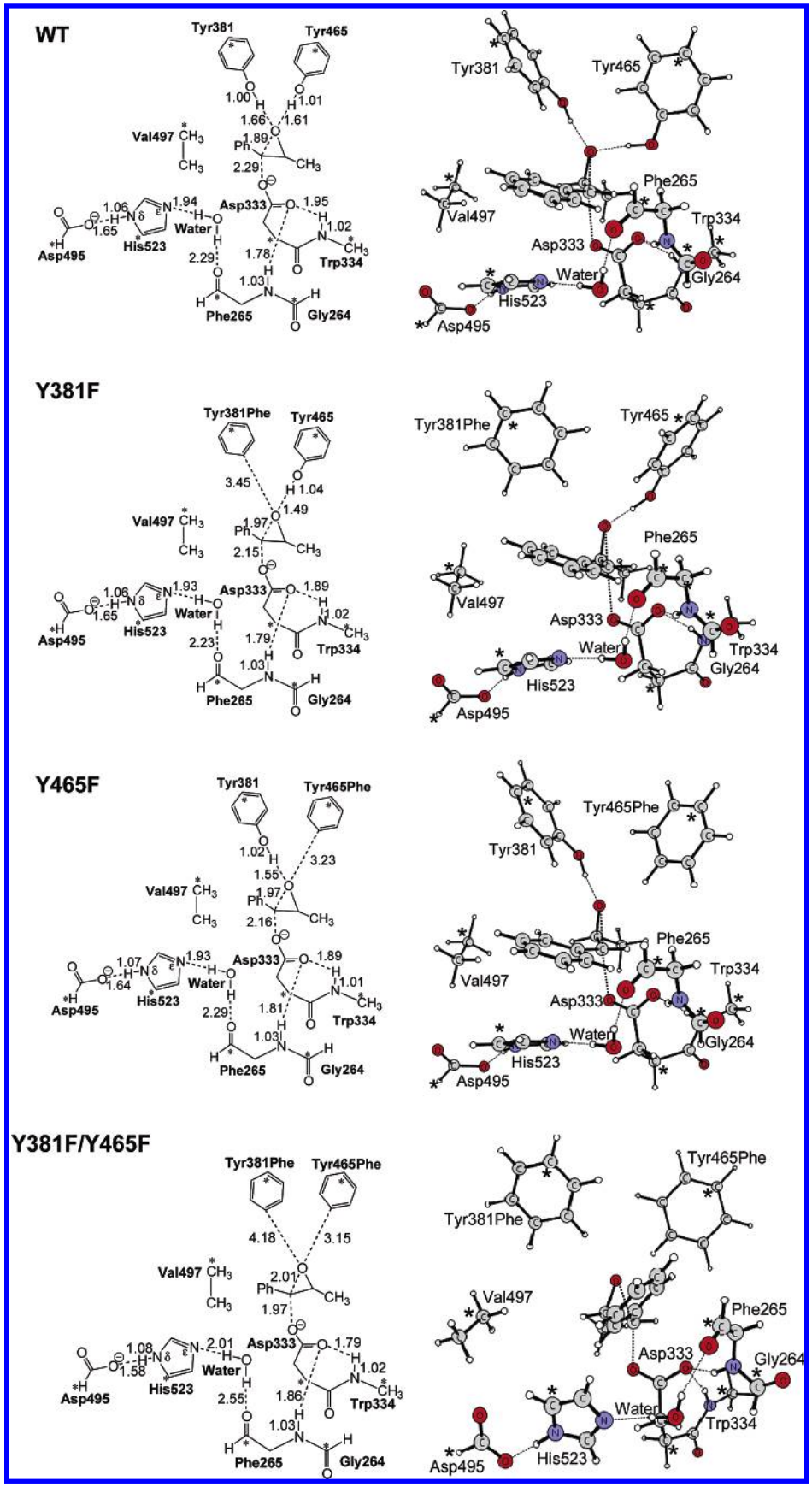

Figure 2. Optimized geometries for the alkylation TS (TSa) for attack at C1 of MSO for the WT, Y381F, Y465F, and Y381F/Y465F models. Detailed information about the structures and the optimized distances (Å) are shown to the left.

to the substrate oxygen is lost, and the emerging negative charge is less stabilized and proton transfer from tyrosine occurs in concert with epoxide opening.

The hydrolytic half-reaction exhibits the same two steps for both the WT model and the single mutant models. In the first step, His523 acts as a general base to activate the catalytic water

TABLE 1: Optimized Transition State Distances (Å) for the Wild-Type and the Tyrosine Mutant Models

TS[a]		Distance	WT	Y381F	Y465F	Y381F/ Y465F	
TSa	**r1**	Asp333Oδ2 to MSO C1	2.29	2.15	2.16	1.97	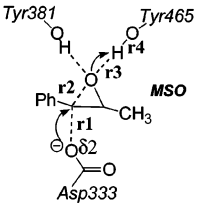
	r2	MSO C1 to MSO O	1.89	1.97	1.97	2.01	
	r3	MSO O to Tyr proton[b]	1.61,1.66[c]	1.49	1.55	-	
	r4	Tyr proton to Tyr O[b]	1.00,1.01[c]	1.04	1.02	-	
TSw	**r5**	Water O to Asp333 C	1.74	1.73	1.76	-	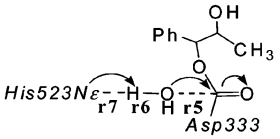
	r6	Water H to water O	1.23	1.23	1.20	-	
	r7	Water H to His523Nε	1.27	1.27	1.30	-	
TSd	**r8**	Diol O to Asp333 C	2.02	2.00	2.07	-	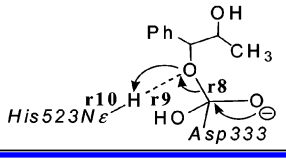
	r9	Diol O to H	1.42	1.37	1.36	-	
	r10	H to His523Nε	1.14	1.17	1.17	-	

[a] TSa = TS alkylation, TSw = TS water attack, TSd = TS dissociation. [b] Tyr465 for Y381F, and Tyr381 for Y465F. [c] Tyr381 and Tyr465, respectively.

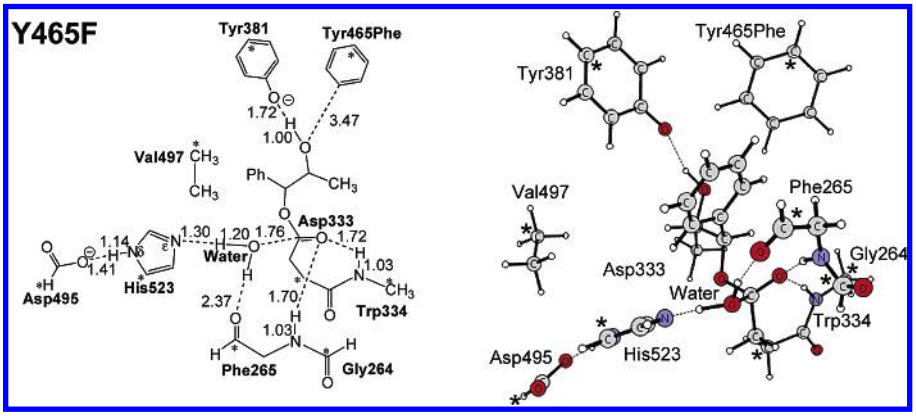

Figure 3. Water attack transition state (TSw) for the Y465F model (attack at C1 of MSO).

molecule, which attacks the Asp333 ester, resulting in formation of a tetrahedral intermediate. The transition state for water attack (TSw) is shown for the Y465F model in Figure 3. At the TS, the water oxygen is 1.76 Å (r5) from the Asp333 carbonyl carbon (Table 1), while the water proton is 1.20 Å (r6) from the water oxygen and 1.30 Å (r7) from His523Nϵ. The three corresponding distances in the Y381F model and the WT model are very similar (Table 1). Concertedly with water attack, we observe in the WT and the single mutant models transfer of a proton from His523Nδ to Asp495. It is possible that this is an artifact of our model and that inclusion of additional residues around Asp495 might stabilize its anionic form and prevent proton transfer. The TS for dissociation of the tetrahedral intermediate (TSd) to yield the final diol product is shown in Figure 4 for the Y465F model. The bond between the Asp333 carbonyl carbon and the oxygen of the emerging diol is broken at 2.07 Å (r8) in the Y465F model (Figure 4). The corresponding r8 distance is 2.00 for Y381F and 2.02 for the WT model (Table 1). In both the WT and the single mutant models, the dissociation is coupled to a simultaneous proton transfer from Nϵ of His523 to the emerging oxyanion of the diol. In the Y465F model, the proton is found 1.36 Å (r9) from the emerging diol oxygen and 1.17 Å (r10) from the Nϵ of His523. The optimized intermediate and product structures for the Y465F model with MSO can be found in Supporting Information (Figure S2A−D). Also, the optimized geometries for the Y381F and the Y381F/Y465F models with MSO are shown in Supporting Information (Figures S1A−F and S3A−B). The geometries of the wild-type model have been reported previously.[21]

B. Energetics of Single and Double Tyrosine Mutants. The overall energy diagrams for the WT and tyrosine mutant models are shown in Figure 5, while in Table 2, the energy barriers for the individual reaction steps for the WT and the mutant models are compared. The first step of the reaction, the alkylation, exhibits the largest difference in energetics between the models. For the WT model, the computed barrier for attack at C1 of MSO is 7.8 kcal/mol.[21] The barrier is 13.2 kcal/mol for the Y465F model and 15.7 kcal/mol for the Y381F model. The alkylation barriers are thus significantly higher for the single mutants than that for the wild-type model. However, the barriers indicate that one tyrosine is still sufficient for the alkylation half-reaction to occur. For the Y381F/Y465F double mutant, the barrier for alkylation is as large as 24.8 kcal/mol. In the double mutant, no proton is available to be transferred to the developing oxyanion, and the high barrier can be explained with a lack of stabilization of the transition state and the formed

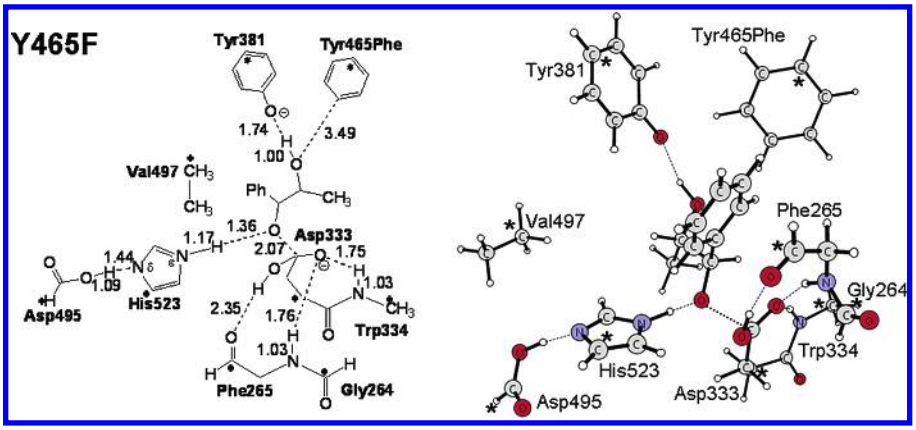

Figure 4. Dissociation transition state (TSd) for the Y465F model (attack at C1 of MSO).

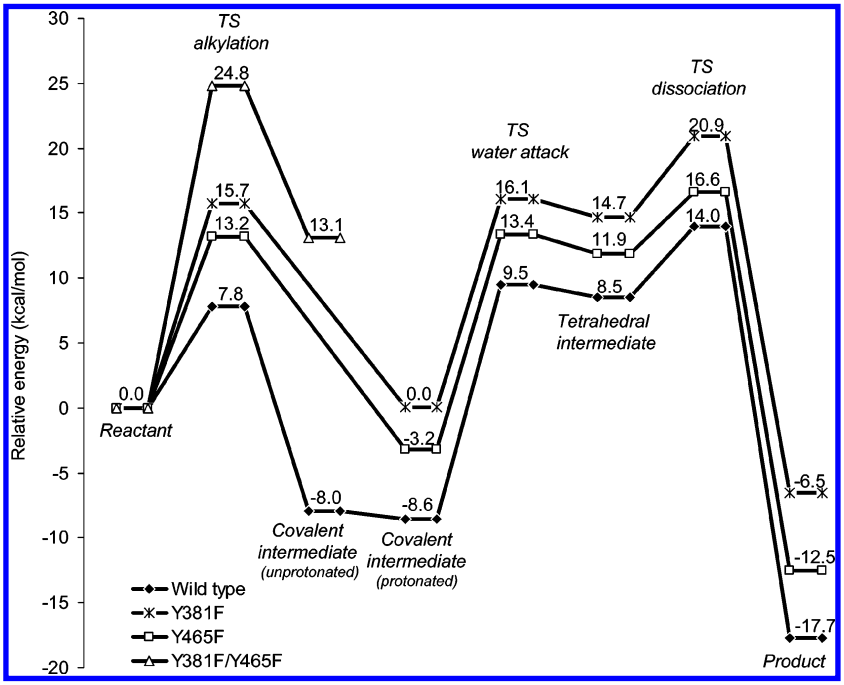

Figure 5. Potential energy diagrams for hydrolysis of MSO (attack at C1). Energetics for the full reaction mechanism are shown for the WT and the single mutant models Y381F and Y465F. For the double mutant Y381F/Y465F, only the energetics for the alkylation step are shown.

TABLE 2: Calculated Barriers (kcal/mol)[a] for MSO Hydrolysis with the Wild-Type and Mutant Models

model	alkylation (TSa)	dealkylation[b]	water attack (TSw)	dissociation (TSd)	overall activation barrier
WT	7.8	16.4	18.1	5.5	22.6
Y381F	15.7	15.7	16.1	6.2	20.9
Y465F	13.2	16.4	16.6	4.7	19.8
Y381F/Y465F	24.8	11.7			

[a] All energies reported here included ZPV and CPCM corrections. [b] The reverse reaction of the reversible alkylation step

covalent intermediate. The calculated value of 24.8 kcal/mol indicates that a double tyrosine mutant would be inactive. Therefore, further reaction steps were not investigated for the double mutant model.

The covalent intermediate (CI) was found to be quite stable in the WT model with a relative energy of −8.6 kcal/mol compared to the reactant (Figure 5).[21] For the single mutant models, the relative energy of the CI is 0.0 and −3.2 kcal/mol for the Y381F and Y465F models, respectively, and +13.1 for the double mutant (Figure 5). The CI is thus much less stable in the mutants than in the WT model. The energetics for the water attack transition state (TSw) are quite similar for the WT and single mutant models, with a barrier of 18.1 kcal/mol for the WT model and 16.1 and 16.6 kcal/mol for the Y381F and Y465F models, respectively (Table 2). For all three models, the tetrahedral intermediate is found only 1.0−1.5 kcal/mol below the TS for water attack (Figure 5). Also, the TSd barriers are similar for the three models, 5.5, 6.2, and 4.7 kcal/mol for the WT, Y381F, and Y465F models, respectively (Table 2). It is interesting to note that the overall barrier for the rate-limiting hydrolytic half-reaction corresponds to 22.6 kcal/mol for the WT model, while it is 20.9 and 19.8 kcal/mol for the Y381F and Y465F models, respectively (Table 2).

C. Comparison to Experimental Results. The computed results for the tyrosine mutant models can be compared to experimental results for a number of different EHs. The kinetic mechanism for the soluble epoxide hydrolases is generally described as in eq 1:[31]

$$E + S \overset{K_s}{\rightleftharpoons} E\bullet S \underset{k_{-2}}{\overset{k_2}{\rightleftharpoons}} E{-}S \xrightarrow{k_3} E + P \qquad (1)$$

(Alkylation: k_2; Dealkylation: k_{-2}; Hydrolysis: k_3)

where E = enzyme, S = substrate, E•S = enzyme−substrate complex, E−S = covalent enzyme−substrate intermediate,

TABLE 3: Numbering of Catalytically Important Residues[a] of EHs Described in the Text

enzyme	catalytic triad[b]	acid catalysts	known Tyr → Phe mutants	ref
rat/mouse/human sEH[c]	D495-H523-D333	Y381 + Y465	Y381F, Y465F, Y381F/Y465F	18
A.radiobacter AD1 EH	D246-H275-D107	Y152 + Y215	Y152F, Y215F, Y152F/Y215F	19
potato EH (StEH1)	D265-H300-D105	Y154 + Y235	Y154F, Y235F, Y154F/Y235F	32
soybean EH	D285-H320-D126	Y175 + Y255	Y255F	33
Aspergillus niger EH	D348-H374-D192	Y251 + Y314	-	4
rat/human microsomal EH	E404-H431-D226	Y374(+Y299?)	Y374F	18

[a] Residues in single letter code, D = aspartate, H = histidine, E = glutamate, Y = tyrosine, F = phenyalanine. [b] In order: charge relay residue−catalytic His−nucleophilic Asp. [c] Tyrosine mutants only made for the mouse sEH.

P = product, K_s = binding constant, k_2 = alkylation rate, k_{-2} = dealkylation rate, and k_3 = rate of the hydrolytic step. The alkylation half-reaction is known to be reversible with $k_2 \gg k_{-2}$. A quite stable covalent E−S intermediate is formed, which can be isolated. The irreversible hydrolytic step is found to be rate limiting for most EHs, with $k_3 \ll k_2$.[19,35,31] Our WT model reproduces these general observations, as discussed previously.[21]

Experimentally, tyrosine mutants have been prepared for a number of different EHs from the α/β-hydrolase fold family. As the catalytic residues are numbered differently depending on the EH, an overview is given in Table 3. Y381F, Y465F, and Y381F/Y465F mutants have been prepared for the mouse sEH.[18] Their analogue mutants of *A. radiobacter* AD1 EH are Y152F, Y215F, and the double mutant Y152F/Y215F.[19,30] For the potato EH, the reported mutants are Y154F, Y235F, and the double mutant Y154F/Y235F.[32] For the soybean EH, a Y255F mutant has been studied.[33] Additionally, a single mutant of human microsomal EH, Y374F, has been reported.[18]

The reported single Y → F mutants for mouse sEH, human microsomal EH, soybean EH, and potato EH all exhibit reduced activities with different substrates compared to the wild-type enzymes.[18,32,33]

For the *A. radiobacter* AD1 EH, the kinetics of the single mutant Y215F and the wild type were compared for hydrolysis of (*R*)-styrene oxide.[19] The experimental rate constant for the alkylation step was found to be $k_2 = 1100\ s^{-1}$ for the wild-type *A. radiobacter* AD1 EH enzyme, which was reduced 18-fold for the Y215F mutant to $k_2 = 60\ s^{-1}$.[19] This corresponds to an increase in the barrier of ca. 1.8 kcal/mol. In our calculations, the barrier increases from 7.8 kcal/mol to 13.2 and 15.7 kcal/mol for the Y465F and Y381F model, respectively, which is a considerable overestimation compared to experiments.[19] A possible reason for this could be the size of the used quantum model. In the active site of the mutants, other polarization effects might compensate for the loss of one hydrogen bond, and the effect of a single tyrosine mutation is therefore less severe than it seems to be in our quantum chemical model. Such specific polarization effects lack the homogeneous CPCM surroundings that are used in our calculations to estimate the effect of the protein surroundings.

Although the alkylation barriers have increased for the single mutants compared to the WT model, the alkylation step has not become rate limiting. This is in agreement with experimental results for the Y251F mutant of *A. radiobacter* AD1 EH, which show that the alkylation rate is reduced, yet not rate limiting.[19] In our calculations, mutation of both tyrosines to phenylalanine leads to an alkylation barrier as large as 24.8 kcal/mol, indicating that a Y381F/Y465 double mutant of human sEH would show very little or no catalytic activity. In agreement with this, virtually no activity is observed for the double tyrosine mutant of *A. radiobacter* AD1 EH, Y152F/Y215F,[19] the potato EH double mutant Y154F/Y235,[32] and the mouse sEH double mutant Y381F/Y465F.[18]

For the hydrolytic half-reaction, we compute an overall activation barrier of 22.6 kcal/mol for the WT model and 19.8 and 20.9 kcal/mol for the Y465F and Y381F models, respectively. These energies are close but indicate a slightly faster hydrolytic step for the single mutants than for the wild type. For the wild-type *A. radiobacter* AD1 EH, the experimental rate constant for the hydrolytic step is found to be $k_3 = 4.2\ s^{-1}$, while the Y251F mutant has a somewhat larger hydrolysis rate of $k_3 = 8.0\ s^{-1}$.[19]

D. Regioselectivity of Epoxide Opening. Nucleophilic attack on an epoxide can in principle occur at two different carbons. An interesting question is whether the regioselectivity of the tyrosine mutants changes compared to the WT model.

To our knowledge, the regioselectivity of epoxide opening has not been studied experimentally with any Tyr → Phe EH mutants. A theoretical study of this aspect can help to gain deeper understanding into the factors that govern the regioselectivity of sEH.

Epoxide opening is normally governed by both steric and electronic factors. Under basic reaction conditions, steric factors are often determining the regioselectivity, leading to attack at the least hindered carbon.[34] Favorable substituents that are able to stabilize the positive charge that develops on the attacked carbon during epoxide opening might shift the regioselectivity and result in attack at the more substituted (and hence usually more hindered) carbon. Presence of an acid catalyst enhances the preference for the more substituted carbon.[34]

In the WT model, the two tyrosines donate one hydrogen bond each to the epoxide oxygen. Although none of the protons is transferred during the alkylation step, it can still be expected that the two hydrogen bonds polarize the O−C bonds of the oxirane ring, resembling an acid-catalyzed reaction. In the single mutant models, Y381F and Y465F, a proton is transferred to the epoxide oxygen from the remaining tyrosine in concert with the nucleophilic attack of Asp333 on the oxirane carbon, that is, the reaction is general acid catalyzed. The double mutant on the other hand has no possible general acid present.

The regioselectivity for MSO hydrolysis was examined by determining the barrier for attack at C2 in the different models and comparing it to the barrier for attack at C1 (the geometries for the alkylation TS for attack at C2 of MSO in all three mutant models are shown in Supporting Information, Figure S4A−C. The geometries of the wild-type model have been reported previously.[21]) Interestingly, for both the mutant and the wild-type models, attack at the benzylic carbon (C1) is favored (Table 4). The difference in barrier for attack at C1 and attack at C2 of MSO ranges from 2.9 to 4.9 kcal/mol for the four models (see Table 4). For all models, epoxide cleavage seems to be determined by electronic factors, also in the absence of a general acid. Experimentally, the regioselectivity of MSO opening has been investigated for mouse sEH,[25] rabbit sEH,[24] and *Aspergillus terreus* EH.[23] Regioselectivity was reported to be 100, 98, and 95 for attack at the benzylic position for the three enzymes, respectively. This agrees well with our theoretical results for

TABLE 4: Regioselectivity of MSO and SSO Opening; Barrier (in kcal/mol)[a] for the Alkylation TS for Attack at C1 (benzylic) or C2 (homobenzylic/terminal)

	MSO			SSO		
model	barrier C1	barrier C2	difference	barrier C1	barrier C2	difference
WT	7.8	11.0	+3.2	6.3	7.0	+0.7
Y465F	13.2	17.4	+4.2	14.0	14.8	+0.8
Y381F	15.7	20.6	+4.9	13.7	15.5	+1.8
Y381F/Y465F	24.8	27.7	+2.9	24.2	23.6	−0.6

[a] All energies reported here included ZPV and CPCM corrections.

SCHEME 2. Possible Mechanism of the Alkylation Half-Reaction as Proposed on the Basis of MD Simulations[37]

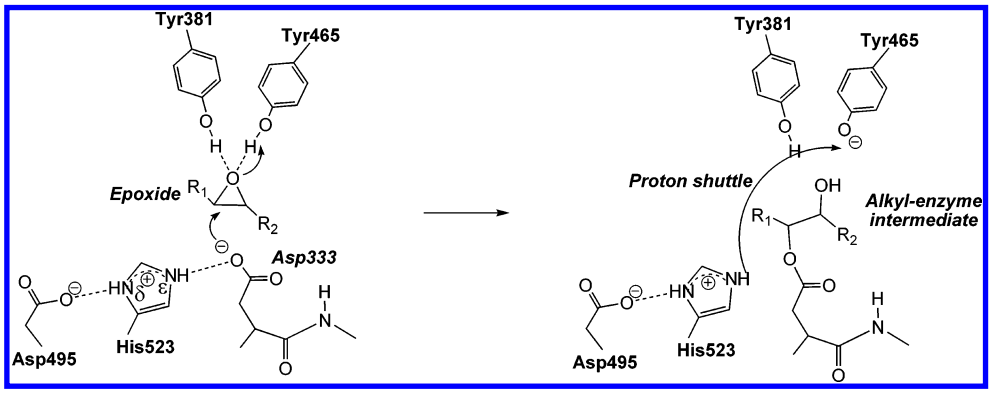

His523 is suggested to be protonated at Nϵ and form a hydrogen bond to Asp333. A proton shuttle is necessary to remove the extra proton on His523 prior to the hydrolytic step.

human sEH, which indicate that attack exclusively occurs at the benzylic position of MSO.

To shed more light on the issue of regioselectivity, we have also studied epoxide opening for another substrate, (*S*)-styrene oxide (SSO). SSO is identical to MSO except that SSO lacks the methyl substituent on C2. Regioselectivity of SSO opening was studied with the WT model and the mutant models Y381F, Y465F, and Y381/Y465. The energetic results are shown in Table 4 (The optimized geometries of the mutant models with SSO can be found in Supporting Information, Figures S5−S7. The geometries of the wild-type model have been shown previously.[21]). For the WT model and the two single mutant models, electronic factors determine the regioselectivity, with preferred attack at the benzylic position (C1). In the double mutant model, steric factors dominate and attack is preferred at the terminal carbon (C2) of SSO. It can be noted, however, that for all models, the differences in barriers for the attack at C1 and C2 for SSO are smaller than that for MSO. With a difference in barriers of less than 2 kcal/mol, it can be assumed that hydrolysis of SSO does not lead to exclusive attack at the preferred carbon but will lead to a mixture of products. This is in agreement with experimental results showing that rabbit sEH-mediated hydrolysis of SSO leads to 45% attack at the benzylic position and 55% attack at the terminal position.[24] For wild-type *A. radiobacter* AD1 EH[35,36] and the rabbit microsomal EH,[24] however, attack seems to occur exclusively at the terminal carbon of SSO. Because epoxide opening is mediated by the same catalytic residues in these enzymes as in human sEH, other differences in the active site must account for the different regioselectivities. It can also be noted from our results that the two single mutant models, Y381F and Y465F, do not give exactly the same results (Table 4). For both substrates (SSO and MSO), Y381F exhibits a stronger preference for the benzylic position (C1) than Y465F does. This indicates that the position of the tyrosine residue that protonates the epoxide oxygen might have some influence on the regioselectivity of epoxide opening.

E. The Importance of His523 for the Alkylation Half-Reaction. The reaction mechanism of sEH presented in Scheme 1 suggests that the catalytic histidine, His523, is only of importance for the hydrolytic half-reaction. Experimental and theoretical data, however, indicate that His523 might play a role in the alkylation step as well. Mutations of the corresponding His300 in the potato EH to alanine, glutamine, or asparagine affect not only the hydrolytic half-reaction but do unexpectedly also result in an impaired alkylation step.[32] The H300N mutant exhibits an alkylation rate (k_2) of 0.3 s^{-1}, which is several orders of magnitude lower than the wild-type potato enzyme (>100 s^{-1}).[32] It has been suggested that the impaired alkylation step of the mutants is due to a loss of activation of the nucleophile Asp105 by His300.[32] This activation is speculated to be mediated by a direct interaction between the two residues.[32] Support for a direct hydrogen bond between the catalytic histidine and the nucleophilic aspartate comes from the crystal structures of the mouse sEH and the *A. radiobacter* AD1 EH,[3,5,6] which implies that the catalytic histidine is protonated at Nϵ. Interestingly, molecular dynamics (MD) studies of the mouse sEH suggest that His523 Nϵ indeed seems to be protonated and that the hydrogen bond formed to Asp333 could be important to keep the later in a favorable orientation for nucleophilic attack on the substrate.[37] The proposed proton on Nϵ of His523, however, has an important consequence. In the hydrolytic half-reaction, the histidine is proposed to act as a general base, abstracting a proton from the catalytic water molecule. If His523 is protonated at Nϵ during the alkylation step, the Nϵ proton has to be removed prior to hydrolysis of the covalent enzyme−substrate intermediate. Therefore, a possible proton shuttle has been suggested, which transfers the proton from Nϵ of His523 to the phenolate of Tyr465 (Scheme 2).[37] The identity of the suggested proton shuttle has to our knowledge not been explored further.

We have investigated what effect a protonation of His523 at Nϵ has on the energetics of the alkylation half-reaction. In the His523NϵH model, His523 was protonated at both Nδ and Nϵ, and the catalytic water molecule was removed. The aim of this model was to study the proposed mechanism as shown in Scheme 2. During the optimization of the reactant species of

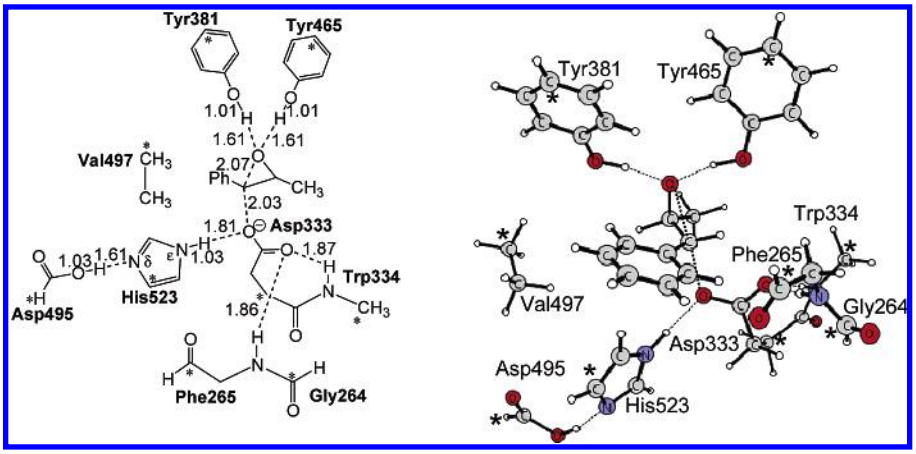

Figure 6. Optimized alkylation TS for attack at C1 in the His523NϵH model.

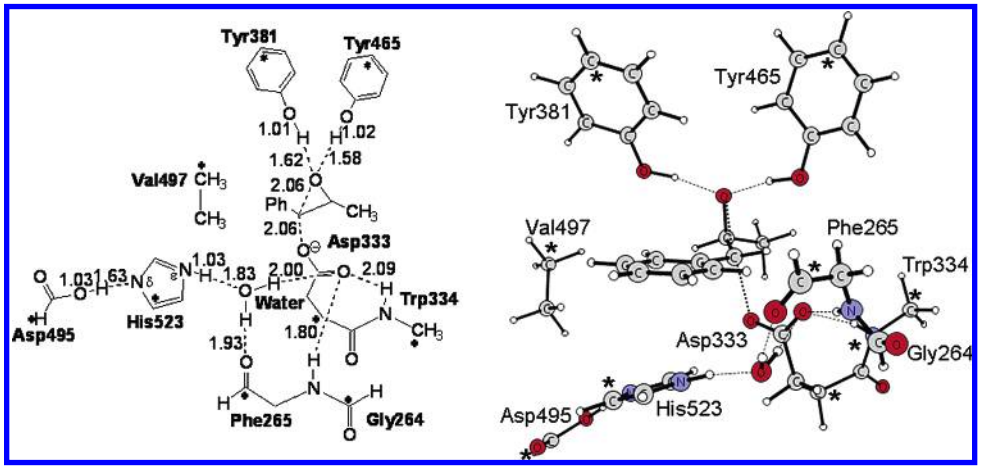

Figure 7. Optimized TS for the alkylation half-reaction for the H523NϵH$-$H$_2$O model.

the His523NϵH model, a hydrogen bond with a length of 2.67 Å was formed between Asp333 Oδ2 and His523 Nϵ (The reactant of the His523NϵH model is shown in Figure S8A, Supporting Information. The hydrogen bond distance refers to the distance between donor and acceptor atoms.). This can be compared to an observed distance of 2.4$-$2.7 Å between Asp333 Oδ2 and His523 Nϵ in the crystal structures of the mouse sEH and the *A. radiobacter* AD1 EH.[3,5,6] The proton placed on Nδ of His523 was transferred to Asp495 during the optimization of the His523NϵH reactant. As noted above, this might be an artifact of the model due to lack of additional residues around Asp495 that stabilize its anionic character. The TS for nucleophilic attack of Asp333 on C1 of MSO in the His523NϵH model was optimized and is shown in Figure 6. The hydrogen bond between Asp333 Oδ2 and His523 Nϵ is preserved in the TS and is found to have a length of 2.84 Å. The distance between Asp333 Oδ2 and the substrate C1 is 2.03 Å. The corresponding distance in the WT model is 2.29 Å. The energy barrier is calculated to be 14.2 kcal/mol, which is 6.4 kcal/mol higher than the barrier calculated for attack on C1 in the WT model (Figure 8). The high barrier can be explained with the hydrogen bond between Asp333 Oδ2 and His523 Nϵ. In the reactant state, this hydrogen bond is rather strong, as it involves interaction with the anionic Asp333 Oδ2 atom. At the alkylation transition state, the anionic character of Asp333 is reduced compared to the reactant state and the length of the hydrogen bond to His523 Nϵ has increased. Reducing the strength of the hydrogen bond in going from the reactant to the TS will be reflected in the calculated barriers, and the His523NϵH model thus exhibits a barrier increase compared to the WT model. A barrier of 14.2 kcal/mol is not so high that a protonated His523 can be completely ruled out.

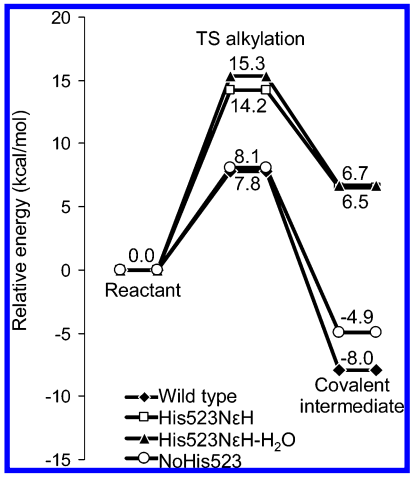

Figure 8. Calculated energetics for the alkylation half-reaction of the His523NϵH, the His523NϵH$-$H$_2$O, and the NoHis523 models.

The covalent intermediate of the His523NϵH model has a relative energy of +6.5 kcal/mol (the structure is shown in Figure S8B, Supporting Information), to be compared to the CI of the WT model, which is $-$8.0 kcal/mol. The high energy of the CI in the His523NϵH model can be explained with the almost complete loss of the hydrogen bond between Nϵ of His523 and Asp333, compared to the reactant state. The hydrogen bond distance is now 3.04 Å and is between two neutral species. It is thus much weaker than the ionic hydrogen

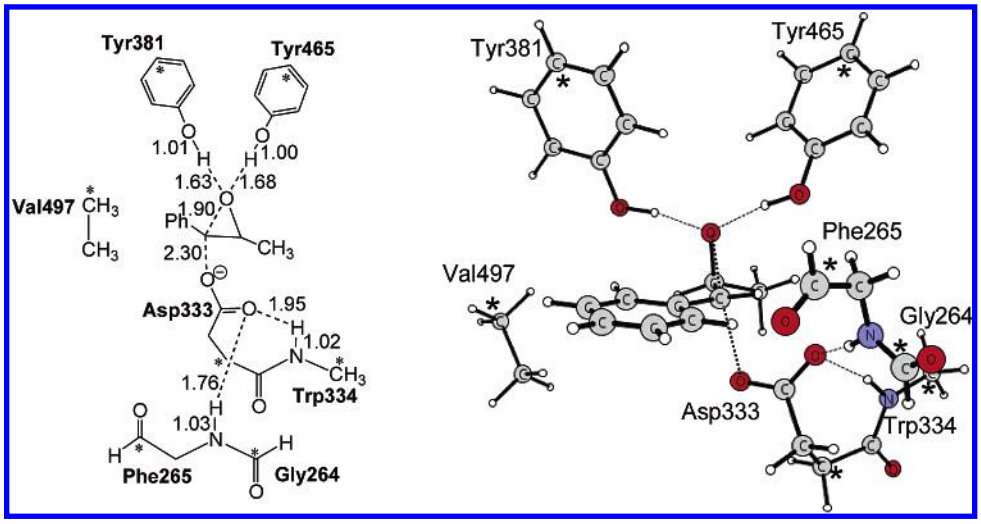

Figure 9. Optimized TS for the alkylation half-reaction for the NoHis523 model.

bond observed in the reactant state. These calculated energies clearly disfavor a protonated histidine model. Experimentally, the CI is known to be relatively stable and to accumulate.[35] The experimental alkylation rate is much larger than the dealkylation rate, that is $k_2 \gg k_{-2}$.[31,35] These experimental results are in line with the WT model, but do not support the His523NϵH model, which exhibits an unstable CI and a barrier for the backward reaction, which is much smaller than for the forward reaction, 7.7 kcal/mol compared to 14.2 kcal/mol.

The catalytic water molecule was excluded in the His523NϵH model, so we decided to prepare an additional model, H523NϵH$-$$H_2O$, which has His523 protonated at Nϵ and the catalytic water molecule present. In the optimized reactant of the H523NϵH$-$$H_2O$ model (shown in Figure S9A, Supporting Information), His523 is protonated at Nϵ, but there is no hydrogen bond to Asp333. Instead, His523 is hydrogen bonded to the oxygen atom of water. The alkylation half-reaction was investigated with this model, and the optimized TS is shown in Figure 7. The barrier for the nucleophilic attack is found to be 15.3 kcal/mol (Figure 8), which is very similar to the barrier found with the H523NϵH model (14.2 kcal/mol). It can be seen in Figure 7 that the water molecule in the H523NϵH$-$$H_2O$ model is involved in hydrogen bonding to the Asp333 Oδ1. Similar to the H523NϵH model, the strength of this hydrogen bond is reduced in going from the reactant to the TS state, which results in an increase of the alkylation barrier. The energy of the unprotonated CI of the H523NϵH$-$$H_2O$ model is +6.7 kcal/mol above the reactant state (the geometry is shown in Supporting Information, Figure S9B), which is very similar to the energy obtained for the CI of the H523NϵH model (+6.5 kcal/mol).

The hydrolytic half-reaction was not investigated with the H523NϵH$-$$H_2O$ model, although the catalytic water molecule was included. Activation of the water molecule by His523 is not possible with His523 protonated at Nϵ. As noted above, the existence of a proton shuttle has been proposed, which would transfer the proton from Nϵ of His523 to Tyr465 (Scheme 2).[37] However, examination of the human sEH structure did not lead to identification of possible residues that could function as such a proton shuttle.

The combined results for the His523NϵH and H523NϵH$-$$H_2O$ model (Figure 8) disfavor a protonation of His523 at Nϵ during the alkylation step, making the proposed mechanism in Scheme 2 unlikely. In agreement with this, experimental data indicate that the catalytic histidine is not protonated during alkylation. For instance, the decrease of catalytic activity of *A. radiobacter* AD1 EH at pH values below 6 has been shown to be due to a single ionization event, suggested to reflect protonation of the catalytic His275.[35] His275 is thus not expected to be protonated in the catalytically active enzyme.[35] Similar results have been obtained for the potato EH[32] and the rat microsomal EH.[12] The origin of the potential hydrogen bond between the nucleophilic aspartate and the catalytic histidine observed in several crystal structures thus remains to be elucidated.[3,5,6] One possibility is that the hydrogen bond is an artifact of the crystallization conditions, as has been suggested for the *A. radiobacter* AD1 EH.[3] This is supported by the observation that there is no indication of an interaction between the catalytic histidine and the nucleophilic aspartate in the structures of the EH from *A. niger* or the human sEH.[4,14]

The impaired alkylation step of the histidine mutants H300N, H300Q, and H300A of the potato EH also remains to be explained.[32] As noted above, it was suggested that the catalytic His300 mediates activation of the nucleophilic aspartate, possibly through a direct hydrogen bond between the two residues.[32] However, pH dependence studies indicate that His300 in the potato EH is not protonated.[32] Moreover, the theoretical results presented here show that if there is a direct hydrogen bond between the nucleophilic aspartate and His300, the alkylation rate is expected to be reduced, not enhanced. Computational models of the histidine mutants might provide further insight into the causes for the reduced alkylation rate. The H300A mutation should be equivalent to a model in which the imidazole side chain of the histidine simply is removed. If the presence of the catalytic histidine indeed is of importance for the alkylation step, then this should be revealed by a chemical model in which His523 is lacking. We prepared a variation of the WT model in which His523 was removed, referred to as the NoHis523 model. Asp495 and the catalytic water were also removed from the NoHis523 model. The TS for nucleophilic attack at C1 of MSO was optimized for the NoHis523 model and is shown in Figure 9 (the reactant can be seen in Figure S10A, Supporting Information). The distance between Asp333 Oδ2 and the C1 of the substrate is found to be 2.30 Å, which is very similar to the WT model (2.29 Å). The barrier for the TS is calculated to be 8.1 kcal/mol, which is almost the same barrier as calculated for the WT model (7.8 kcal/mol, Figure 8). The unprotonated CI formed after nucleophilic attack is found at a relative energy of $-$4.9 kcal/mol (Figure S10B, Supporting Information). Our theoretical results indicate that removal of the catalytic histidine does not seem to have any

effect on the alkylation barrier. This is in contrast to the experimental results obtained for the potato EH,[32] and the underlying cause for the impaired alkylation rate of the catalytic His300 mutants of the potato EH remains to be elucidated. On the basis of the above results, we suggest that, in the wild-type EH enzyme, no hydrogen bond exists between His523 and Asp333. In the His300N and His300Q mutants, however, the introduction of artificial hydrogen bonds between the mutated residues and Asp333 could be the reason for the impaired activity. This would not be expected in a His300A mutant. However, because the small side chain of A300 might make room to allow for additional water molecules to enter the active site, these could hydrogen bond to the anionic Asp333 and reduce its nucleophilic potential. Interestingly, other EHs do not exhibit a 1000-fold decrease in alkylation rate if the catalytic histidine is mutated. In the H413S mutant of rat microsomal EH, the rate of the alkylation step is only reduced 6-fold.[38] This is in line with the theoretical results we obtain for the NoHis523 model.

Conclusions

Single and double mutants of the two conserved active site tyrosines of soluble epoxide hydrolase (sEH) were studied theoretically. The results confirm the importance of the two tyrosines for the alkylation step. The computed alkylation barriers of the single tyrosine mutants Y381F and Y465F are increased significantly compared to the wild-type (WT) model. The two tyrosines are thus acting in concert to lower the alkylation barrier. Although the calculated barriers indicate that loss of one tyrosine might be acceptable, the double mutant model Y381F/Y465F exhibits an alkylation barrier that is so high that no catalytic activity is expected. These results are in line with experimental observations for several epoxide hydrolases.[18,19,32] The mechanism for the hydrolytic half-reaction is identical between the single mutants and the WT model, and the barriers are found to be quite similar, which is also in line with experimental observations.[19] The Tyr → Phe mutant models thus reproduce experimental trends, and it can be concluded that despite the smallness of the models used, calculations on active site mutants can give a good indication of the importance of a residue for the reaction mechanism.

The regioselectivity of epoxide opening was investigated for the substrates (1*S*,2*S*)-β-methylstyrene oxide (MSO) and (*S*)-styrene oxide (SSO) for the WT and the single and double tyrosine mutant models. Attack at the benzylic position (C1) of MSO and SSO is favored for both the WT and the single mutants. For MSO, the difference in barriers implies that exclusive attack at C1 is expected, as observed experimentally for different EHs.[23−25] The preference for the benzylic position is much less for SSO, indicating that for this substrate, a mixture of products is obtained, in agreement with experimental results for rabbit sEH.[24] The double mutant Y381F/Y465F model exhibits preferred attack at the benzylic carbon (C1) of MSO, indicating that attack here is electronically favored also in absence of a general acid. For SSO, the double mutant shows preferred attack at the terminal carbon (C2), which indicates that steric factors dominate the regioselectivity for this substrate in absence of a general acid.

The role of the catalytic histidine in the alkylation half-reaction was also explored in the present study. A proposed protonation of His523 at Nϵ, which leads to a hydrogen bond to the nucleophilic Asp333, was examined and found to be unlikely. As some experimental results indicate an importance of the catalytic histidine for the alkylation step, a model without His523 was investigated as well. The model lacking His523 exhibits energetics that are very similar to the WT model. Thus, an important role for His523 in the alkylation step could not be confirmed.

Acknowledgment. We gratefully acknowledge financial help from The Swedish Research Council, The Wenner−Gren Foundations, The Carl Trygger Foundation, and The Magn Bergvall Foundation.

Supporting Information Available: Optimized geometries for the mutant models Y381F, Y465F, Y381F/Y465F with substrates MSO and SSO; optimized geometries for the H523NϵH, H523NϵH−H_2O, and NoHis523 models; table containing the energy breakdown. This material is available free of charge via the Internet at http://pubs.acs.org.

References and Notes

(1) Morisseau, C.; Hammock, B. D. *Annu. Rev. Pharmacol. Toxicol.* **2005**, *45*, 311−333.
(2) Lacouciere, G. M.; Armstrong, R. N. *Chem. Res. Toxicol*. **1994**, 7, 121−124.
(3) Nardini, M.; Ridder, I. S.; Rozeboom, H. J.; Kalk, K. H.; Rink, R.; Janssen, D. B.; Dijkstra, B. W. *J. Biol. Chem.* **1999**, *274*, 14579−14586.
(4) Zou, J.; Hallberg, B. M.; Bergfors, T.; Oesch, F.; Arand, M.; Mowbray, S. L.; Jones, T. A. *Structure* **2000**, *8*, 111−122.
(5) Argiriadi, M. A.; Morisseau, C. M.; Goodrow, M. H.; Dowdy, D. L.; Hammock, B. D.; Christianson, D. W. *J. Biol. Chem.* **2000**, *275*, 15265−15270.
(6) Argiriadi, M. A.; Morisseau, C.; Hammock, B. D.; Cristianson, D. W. *Proc. Natl. Acad. Sci. U.S.A.* **1999**, *96*, 10637−10642.
(7) Arand, M.; Grant, D. F.; Beetham, J. K.; Friedberg, T.; Oesch, F.; Hammock, B. D. *FEBS Lett.* **1994**, 338, 251−256.
(8) Pinot, F.; Grant, D. F.; Beetham, J. K.; Parker, A. G.; Borhan, B.; Landt, S.; Jones, A. D.; Hammock, B. D. *J. Biol. Chem.* **1995**, *270*, 7968−7974.
(9) Arand, M.; Wagner, H.; Oesch, F. *J. Biol. Chem.* **1996**, *271*, 4223−4229.
(10) Laughlin, L. T.; Tzeng, H.-F.; Lin, S.; Armstrong, R. N. *Biochemistry* **1998**, *37*, 2897−2904.
(11) Rink, R.; Fennema, F.; Smids, M.; Dehmel, U.; Janssen, D. B. *J. Biol. Chem.* **1997**, *272*, 14650−14657.
(12) Bell, P. A.; Kasper, C. B. *J. Biol. Chem.* **1993**, *268*, 14011−14017.
(13) Laughlin, L. T.; Tzeng, H.-F.; Lin, S.; Armstrong, R. N. *Biochemistry* **1998**, *37*, 2897−2904.
(14) Gomez, G. A., Morisseau, C.; Hammock, B. D.; Christianson, D. W. *Biochemistry* **2004**, *43*, 4716−4723.
(15) Newman, J. W.; Morisseau, C.; Hammock, B. D. *Prog. Lipid Res.* **2005**, *44*, 1−51.
(16) Fretland, A. J.; Omiecinski, C. J. *Chem.-Biol. Interact.* **2000**, *129*, 41−59.
(17) Armstrong, R. N.; Cassidy, C. S. *Drug Metab. Rev.* **2000**, *32*, 327−338
(18) Yamada, T.; Morisseau, C.; Maxwell, J. E.; Argiriadi, M. A.; Christianson, D. W.; Hammock, B. D. *J. Biol. Chem.* **2000**, *275*, 23082−23088.
(19) Rink, R.; Kingma, J.; Lutje Spelberg; J. H.,; Janssen, D. B. *Biochemistry* **2000**, 39, 5600−5613.
(20) Mowbray, S. L.; Elfström, L. T.; Ahlgren, K. M.; Andersson, C. E.; Widersten, M. *Protein Sci.* **2006**, *15*, 1−10.
(21) Hopmann, K. H.; Himo, F. A Theoretical Study of the Full Reaction Mechanism of Human Soluble Epoxide Hydrolase. *Chem.—Eur. J.* **2006**, *12*, 6898−6909.
(22) Elfström, L. T.; Widersten, M. *Biochemistry* **2006**, *45*, 205−212.
(23) Moussou, P.; Archelas, A.; Baratti, J.; Furstoss, R. *J. Mol. Catal. B* **1998**, *5*, 213-217.
(24) Bellucci, G.; Chiappe, C.; Cordoni, A.; Marioni, F. *Tetrahedron Lett.* **1994**, *35*, 4219−4222.
(25) Williamson, K. C.; Morisseau, C.; Maxwell, J. E.; Hammock. B. D. *Tetrahedron: Asymmetry* **2000**, *11*, 4451−4462.
(26) (a) Himo, F.; Siegbahn, P. E. *Chem. Rev.* **2003**, *103*, 2421−2456. (b) Siegbahn, P. M.; Borowski, T. *Acc. Chem. Res.* **2006**, http://dx.doi.org/10.1021/ar050123u. (c) Siegbahn, P. E. M. *Q. Rev. Biophys.* **2003**, *36*, 91−145. (d) Cerqueira, N. M. F. S. A.; Fernandes, P. A.; Eriksoon, L. A.; Ramos, M. J. *J. Mol. Struct. (THEOCHEM)* **2004**, *709*, 53−65. (e) Pereira, S.; Cerquerira, N. M. F. S. A.; Fernandes, P. A.; Ramos, M. J. *Eur. Biophys. J.* **2006**, *35*, 125−135. (f) Himo, F. *Biochim. Biophys. Acta* **2005**, *1707*, 24−33. (g) Noodleman, L.; Lovell, T.; Han, W.-G.; Li, J.; Himo, F. *Chem.*

Rev. **2004**, *104*, 459−508. (h) Leopoldini, M.; Russo, N.; Toscano, M. *J. Phys. Chem. B* **2006**, 110, 1063−1072.

(27) (a) Lee, C.; Yang, W.; Parr, R. G. *Phys. Rev. B* **1988**, *37*, 785−789. (b) Becke, A. D. *Phys. Rev. A* **1988**, *38*, 3098−3100. (c) Becke, A. D. *J. Chem. Phys.* **1992**, *96*, 2155−2160. (d) Becke, A. D. *J. Chem. Phys.* **1992**, *97*, 9173−9177. (e) Becke, A. D. *J. Chem. Phys.* **1993**, *98*, 5648−5652.

(28) Frisch, M. J.; Trucks, G. W.; Schlegel, H. B.; Scuseria, G. E.; Robb, M. A.; Cheeseman, J. R.; Montgomery, J. A., Jr.; Vreven, T.; Kudin, K. N.; Burant, J. C.; Millam, J. M.; Iyengar, S. S.; Tomasi, J.; Barone, V.; Mennucci, B.; Cossi, M.; Scalmani, G.; Rega, N.; Petersson, G. A.; Nakatsuji, H.; Hada, M.; Ehara, M.; Toyota, K.; Fukuda, R.; Hasegawa, J.; Ishida, M.; Nakajima, T.; Honda, Y.; Kitao, O.; Nakai, H.; Klene, M.; Li, X.; Knox, J. E.; Hratchian, H. P.; Cross, J. B.; Bakken, V.; Adamo, C.; Jaramillo, J.; Gomperts, R.; Stratmann, R. E.; Yazyev, O.; Austin, A. J.; Cammi, R.; Pomelli, C.; Ochterski, J. W.; Ayala, P. Y.; Morokuma, K.; Voth, G. A.; Salvador, P.; Dannenberg, J. J.; Zakrzewski, V. G.; Dapprich, S.; Daniels, A. D.; Strain, M. C.; Farkas, O.; Malick, D. K.; Rabuck, A. D.; Raghavachari, K.; Foresman, J. B.; Ortiz, J. V.; Cui, Q.; Baboul, A. G.; Clifford, S.; Cioslowski, J.; Stefanov, B. B.; Liu, G.; Liashenko, A.; Piskorz, P.; Komaromi, I.; Martin, R. L.; Fox, D. J.; Keith, T.; Al-Laham, M. A.; Peng, C. Y.; Nanayakkara, A.; Challacombe, M.; Gill, P. M. W.; Johnson, B.; Chen, W.; Wong, M. W.; Gonzalez, C.; Pople, J. A. *Gaussian 03*; Gaussian, Inc.: Wallingford, CT, 2004.

(29) (a) Klamt, A.; Schüürmann, G., *J. Chem. Soc., Perkin Trans.* **1993**, *2*, 799−805. (b) Andzelm, J.; Kölmel, C.; Klamt, A. *J. Chem. Phys.* **1995**, *103*, 9312−9320. (c) Barone, V.; Cossi, M. *J. Phys. Chem. A* **1998**, *102*, 1995−2001. (d) Cossi, M.; Rega, N.; Scalmani, G.; Barone, V. *J. Comput. Chem.* **2003**, *24*, 669−681.

(30) Rink, R.; Lutje Spelberg, J. H.; Pieters, R. J.; Kingma, J.; Nardini, M.; Kellogg, R. M.; Dijkstra, B. W.; Janssen, D. B. *J. Am. Chem. Soc.* **1999**, *121*, 7417−7418.

(31) Tzeng, H.-F.; Laughlin, L. T.; Lin, S.; Armstrong, R. N. *J. Am. Chem. Soc.* **1996**, *118*, 9436−9437.

(32) Elfström, L. T.; Widersten, M. *Biochem. J.* **2005,** *390*, 633−640.

(33) Blée, E.; Summerer, S.; Flenet, M.; Rogniaux, H.; Van Dorsselaer, A.; Schuber, F. *J. Biol. Chem.* **2005**, *280*, 6479−6487.

(34) Clayden, J.; Greeves, N.; Warren, S.; Wothers, P. *Organic Chemistry*; Oxford University Press: New York, 2001.

(35) Rink, R.; Janssen, D. B.. *Biochemistry* **1998**, *37*, 18119−18127.

(36) Lutje Spelberg, J. H.; Rink, R.; Kellogg, R. M.; Janssen, D. B. *Tetrahedron: Asymmetry* **1998**, *9*, 459−466.

(37) Schiøtt, B.; Bruice, T. C. *J. Am. Chem. Soc.* **2002**, *124*, 14558−14570.

(38) Tzeng, H.-F.; Laughlin, L. T.; Armstrong, R. N. *Biochemistry* **1998**, *37*, 2905−2911.